ACS NANO
Cite This: ACS Nano 2018, 12, 3360−3368
www.acsnano.org

ARTICLE

High-Performance All-Solid-State Na−S Battery Enabled by Casting−Annealing Technology

Xiulin Fan,[†,§] Jie Yue,[†,§] Fudong Han,[†] Ji Chen,[†] Tao Deng,[†] Xiuquan Zhou,[‡] Singyuk Hou,[†] and Chunsheng Wang*[,†]

[†]Department of Chemical and Biomolecular Engineering and [‡]Department of Chemistry and Biochemistry, University of Maryland, College Park, Maryland 20742, United States

Supporting Information

ABSTRACT: Room-temperature all-solid-state Na−S batteries (ASNSBs) using sulfide solid electrolytes are a promising next-generation battery technology due to the high energy, enhanced safety, and earth abundant resources of both sodium and sulfur. Currently, the sulfide electrolyte ASNSBs are fabricated by a simple cold-pressing process leaving with high residential stress. Even worse, the large volume change of S/Na_2S during charge/discharge cycles induces additional stress, seriously weakening the less-contacted interfaces among the solid electrolyte, active materials, and the electron conductive agent that are formed in the cold-pressing process. The high and continuous increase of the interface resistance hindered its practical application. Herein, we significantly reduce the interface resistance and eliminate the residential stress in Na_2S cathodes by fabricating Na_2S-Na_3PS_4-CMK-3 nanocomposites using melting-casting followed by stress-release annealing-precipitation process. The casting−annealing process guarantees the close contact between the Na_3PS_4 solid electrolyte and the CMK-3 mesoporous carbon in mixed ionic/electronic conductive matrix, while the *in situ* precipitated Na_2S active species from the solid electrolyte during the annealing process guarantees the interfacial contact among these three subcomponents without residential stress, which greatly reduces the interfacial resistance and enhances the electrochemical performance. The *in situ* synthesized Na_2S-Na_3PS_4-CMK-3 composite cathode delivers a stable and highly reversible capacity of 810 mAh/g at 50 mA/g for 50 cycles at 60 °C. The present casting−annealing strategy should provide opportunities for the advancement of mechanically robust and high-performance next-generation ASNSBs.

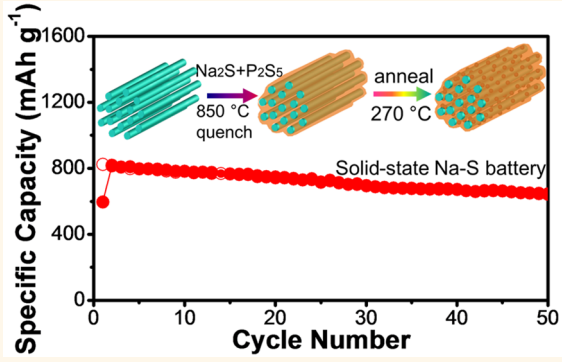

KEYWORDS: *Na−S batteries, solid-state electrolyte, Na_3PS_4, casting−annealing, Na_2S*

As the environmental crisis is becoming more and more serious due to the rapid consumption of fossil fuel in the world, energies obtained from the renewable sources like wind, tide, and solar are escalating. Efficient large-scale energy storage technologies are urgently needed for these renewable energies. Although the lithium-ion batteries (LIBs) have been successfully adopted in the field of the portable electronic devices, the limited and localized natural abundance of Li and safety issues make the commercial LIBs not practical for grid-scale energy storage.[1−4]

For grid-scale energy storage applications, the batteries should meet several critical requirements, in which safety, high-energy density, and natural abundance with low cost are the most important criteria.[1] A sodium−sulfur (Na−S) battery with sulfur or Na_2S as the cathode and sodium or low potential alloys as anode is one of the most promising devices for grid-scale energy storage due to high-energy density, low cost, and readily available resources.[5,6] A high-temperature (>300 °C) Na−S battery has been adopted for large-scale energy storage,[7,8] where an operating temperature of >300 °C is required (1) to lower the interface resistance by keeping the sodium anode and sulfur cathode in liquid state and (2) to increase the Na^+ ion conductivity of solid electrolyte ($NaAl_{11}O_{17}$). During operation, all of the active materials have to be in the molten state, therefore only Na_2S_x ($x \geq 3$) species with melting points <300 °C are allowed to be generated during the sodiation (discharge) process, limiting to one-third (~760 Wh/kg) of the theoretical energy density released.[9,10] Besides, the molten state of the electrodes will dramatically increase the reactivity at high temperatures,[11]

Received: December 15, 2017
Accepted: March 16, 2018
Published: March 16, 2018

DOI: 10.1021/acsnano.7b08856
ACS Nano 2018, 12, 3360−3368

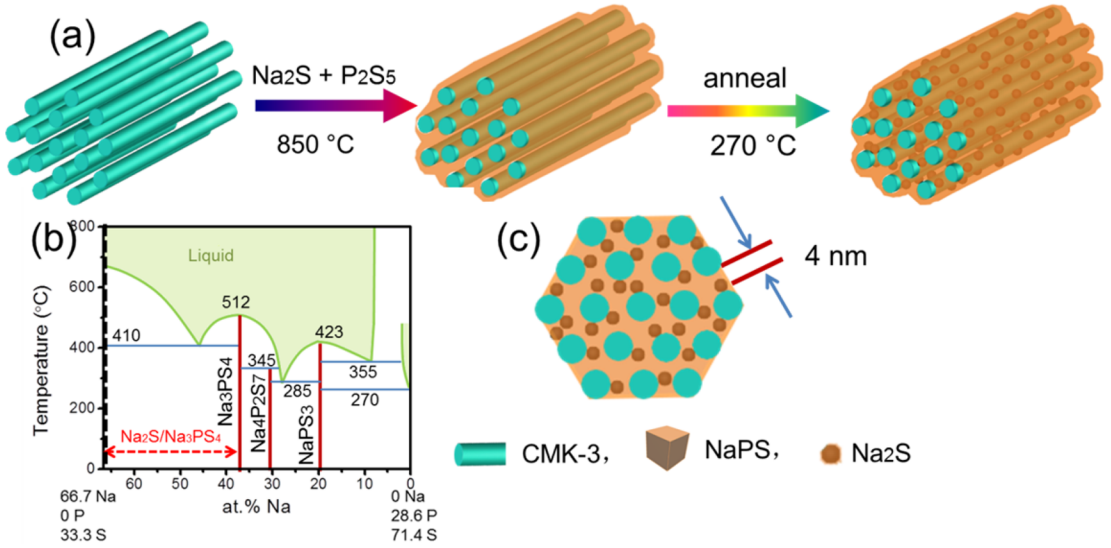

Figure 1. (a) Schematic illustration of the synthesis of cast-annealed Na_2S-NPS-C composite cathode. (b) Phase diagram of the Na_2S and P_2S_5. (c) The front-view of a single rod of the cast-annealed Na_2S-NPS-C composite.

bringing serious safety issues.[12] Any fracture of the brittle solid-state electrolyte will induce a fire or even an explosion at this temperature.[8] Therefore, the high operational cost, safety concerns, and maintenance issues limit the high-temperature Na−S batteries' widespread applications.

Inspired by the successful room-temperature Li−S batteries,[13] intensive investigations have been conducted to develop a low-temperature Na−S battery using liquid organic-based electrolytes,[14−25] polymer electrolytes,[26,27] or liquid−solid hybrid electrolyte.[6] In the liquid-electrolyte batteries, the fluid electrolyte can penetrate into the pores of the electrodes to guarantee the ion conductive pathways and flow back/forward from porous electrode to meet the volumetric change of the materials during charge and discharge cycles. Such merits are also held in the high-temperature Na−S battery. The intimate contact between the liquid electrolyte and the electrode materials and high capability to accommodate the volumetric change of the electrode materials in the liquid electrolyte Na−S battery enhance the ionic conductivity and charge transfer and cycle life. However, liquid electrolyte Na−S batteries also suffer the shuttle reactions as do the Li−S batteries,[14,20,28] and the safety issues due to the flammability of the electrolyte and the formation of sodium dendrites in cycling limit the application for the large-scale energy storage.[29] The ultimate solution of the safety issue for Na−S battery lies in the development of a low-temperature all-inorganic solid-state Na−S battery (ASNSB), in which the inorganic solid−electrolyte is intrinsically nonflammable. Despite of the great promises, the performance of ASNSBs still suffers from the huge electrode/electrolyte interfacial resistance.[30] Different from the interfacial contact between solid and liquid in the room-temperature liquid electrolyte or high-temperature liquid electrode Na−S cells, the contact between the all-solid electrolyte and the solid electrodes is point-to-point due to the nature of nonfluidity and rigidity for the solid electrodes and the electrolyte, thereby the interfacial resistance experiences an exponential increase during charge/discharge cycles. Any cracks formed due to the volume change during sodiation and desodiation will make the acive material detach from the solid electrolyte and/or electron conducting agent, leading to the fast deterioration of the electrochemical reversibility.[31] Therefore, only limited success with poor cycling performance was reported in the ASNSBs.[9,32,33] Recently, our group demonstrated that the reversibility of the ASNSB can be enhanced by decreasing the particle size of Na_2S into nanometers by ball-milling. However, the high residential stress and poor interface contact induced by cold-pressing still limit the cycling stability. Therefore, the reversible capacity still quickly drops to ∼50% of the initial reversible capacity after only 50 cycles.[32] A high-performace ASNSB can be realized, only if the active materials of S/Na_2S, solid electrolyte, and electronic conducting agent are homogeneously distributed in the cathode with nanoscaled stress-free triple-phase contact for rapid charge-transfer reactions and meanwhile possess a mechanically robust structure to sustain the large volume change during sodiation/desodiation.

Cast-annealing process is one of the most mature methods for fabricating the structural materials with high mechanical and physical properties. This facile method possesses several merits: (1) the tension/stress will be eliminated during the precipitation process of heat treatment; (2) the precipitates from the matrix are thermodynamically stable; and (3) *in situ* precipitated phases partially coherent with the parent materials reduce the interface resistance and enhance the mechanical property. Therefore, the structural materials synthsized by this facile method have been extensively adopted in automotive and aerospace industries because of their ideal castability, good corrosion resistance, and improved mechanical properties in the severe working conditions.[34,35] Herein, inspired by the facile and sustainable casting−annealing and precipitation approach in the metal production, we designed and synthesized a robust Na_2S-Na_3PS_4-CMK-3 (denoted as cast-annealed Na_2S-NPS-C) composite cathode for ASNSB, in which Na_2S nanoparticles are homogeneously precipitated from the solid electrolyte during annealing of quenched Na_2S-P_2S_5-CMK-3 composites. The uniformly distributed Na_2S active nanoparticles with low interface resistance with parent Na_3PS_4 solid electrolyte can enhance the mechanical strength and the capability to accommodate the volumetric change of Na_2S active materials in the sodiation and desodiation cycles. The ASNSB using an *in situ* synthesized cast-annealed Na_2S-NPS-C nanocomposite cathode delivered a high reversible capacity of about 700

DOI: 10.1021/acsnano.7b08856
ACS Nano 2018, 12, 3360−3368

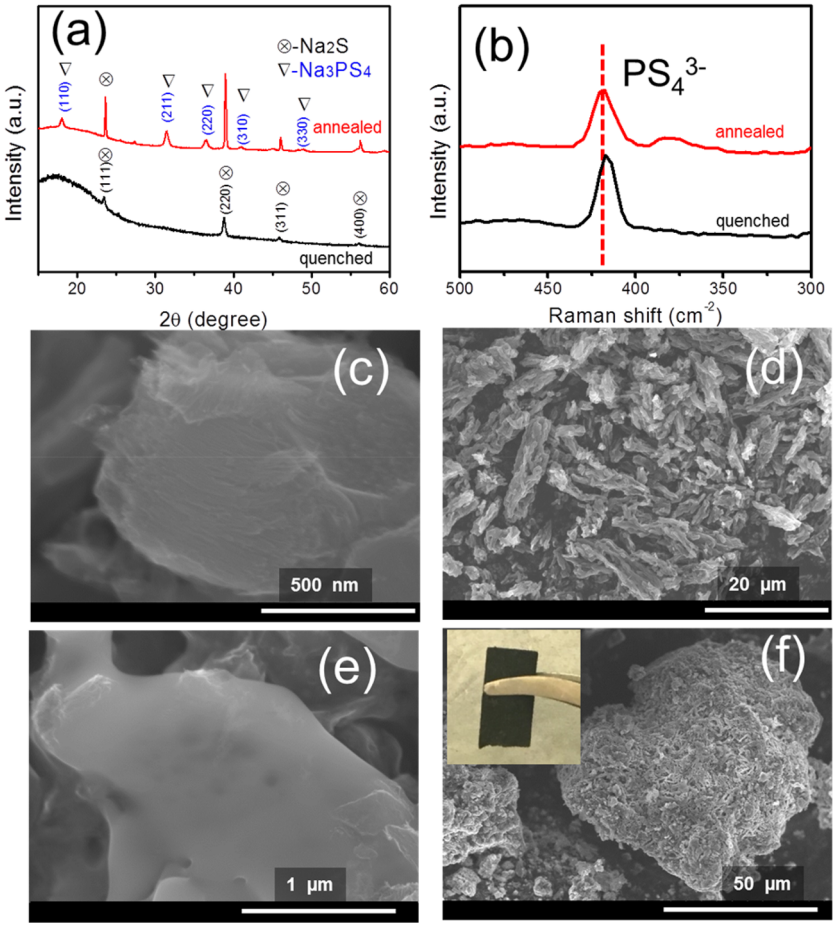

Figure 2. (a) XRD patterns of quenched Na_2S/Na_3PS_4/CMK-3 composite before and after annealing. (b) Raman spectra of the quenched composite and the annealed composite. (c) and (d) SEM images of the CMK-3 mesoporous carbon. (e) and (f) SEM images of the annealed composite. The inset in (f) shows the optical image of as-synthesized cast-annealed Na_2S-NPS-C nanocomposite.

mAh/g at 60 °C for over 50 cycles. Use of mature synthesis method of structural composite material to fabricate functional battery materials opens up opportunities in the exploration of ASNSB for high-performance next-generation Na−S batteries.

RESULTS AND DISCUSSION

Figure 1 demonstrates a schematic illustration for the *in situ* synthesis of the cast-annealed Na_2S-NPS-C composite materials. In brief, the starting materials of Na_2S, P_2S_5, and CMK-3 mesoporous carbon were hand milled with mortar and pestle in the glovebox. The mixtures were then transferred into a graphite crucible, which was then put into a quartz tube and sealed under vacuum (Figure S1). As the temperature was raised to higher than the liquidus (phase diagram, Figure 1b),[36,37] the Na_2S and P_2S_5 melted with each other, forming a homogeneous liquid. The melting liquid in the sealed quartz tube was then quenched by quickly transferring it into the ice water mixture. After quenching, the composite was annealed at 270 °C for 2 h, during which the Na_2S nanoparticles would *in situ* precipitate from the electrolyte-carbon composite. Figure 1c shows the front view of a single rod of the as-formed Na_2S-NPS-C composite. All of the meso-channels (4 nm) in the CMK-3 were filled with the Na_2S and Na_3PS_4 composite. The ratio among Na_2S active material and Na_3PS_4 electrolyte can be adjusted based on the Na_2S-P_2S_5 phase diagram (Figure 1b) through changing the ratio of the starting materials of Na_2S and P_2S_5, while the nanoscaled electronic and ionic conductivity of Na_2S-Na_3PS_4-CMK-3 cathodes can be balanced by adjusting the ratio of Na_2S-P_2S_5 to CMK-3. The adjusting areas have been denoted in the phase diagram with a double-head-arrow dash line, and the concentration of Na_2S and Na_3PS_4 in the final products can be determined based on the lever rules. One of the merits for this technique is that the solid electrolyte and the active species can be *in situ* precipitated from the simple starting materials of Na_2S and P_2S_5, forming a stable interface with a low interfacial resistance and interfacial stress/strain while the liquid Na_2S and P_2S_5 at high temperature wet with CMK-3, all of which ensure perfect contacts among the solid electrolyte, electron conducting agent, and the active species, therefore maximizing the utilization of the Na_2S species. Besides, using the presodiated Na_2S as the cathode active species could provide enough space for the volumetric change of the electrode during sodiation/desodiation reactions.

Figure 2a shows the XRD patterns of the quenched Na_2S/Na_3PS_4/CMK-3 composite before and after heat-treating at 270 °C for 2 h. For the quenched sample, several small peaks can be observed, which can be well indexed to the (111), (220), (311), and (400) of Na_2S (JCPDS no. 23-0441). The formation of these tiny crystalline Na_2S is possibly due to the ready crystallization during the quenching process. After heat-treating at 270 °C for 2 h, the peak intensity of Na_2S was dramatically increased along with the appearance of new peaks from crystallization of Na_3PS_4 phase. The unusual background between 10° and 30° arises from amorphous scattering caused

DOI: 10.1021/acsnano.7b08856
ACS Nano 2018, 12, 3360−3368

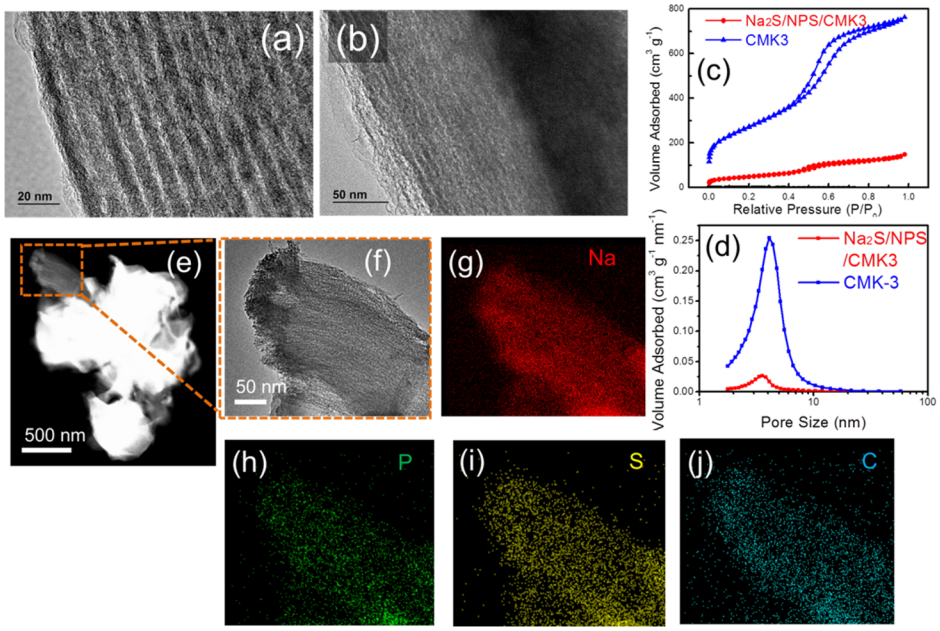

Figure 3. TEM image of the CMK-3 (a) and the as-synthesized cast-annealed Na_2S-NPS-C nanocomposite (b). N_2 adsorption/desorption isotherm of the mesoporous carbon (CMK-3) and the as-synthesized cast-annealed Na_2S-NPS-C nanocomposite (c) and the corresponding BJH pore size distribution curves (d). (e) STEM-HAADF image of the cast-annealed Na_2S-NPS-C nanocomposite; (f) enlargement of the figure (e) (TEM image) and the corresponding elemental mapping Na (g), P (h), S (i), and C (j).

by the Kapton film used to seal the sample during XRD characterization. XRD patterns of the ball-milled Na_2S/NPS (Figure S2) and Na_2S-NPS-C composite (Figure S3) show only Na_3PS_4 and Na_2S phases. No any impurities can be detected in both samples.

Raman spectra of the quenched and the annealed Na_2S-Na_3PS_4-CMK-3 composites are shown in Figure 2b. The Raman spectroscopy reveals that the thiophosphate ions have been formed in the melting process and preserved after quenching as evidenced by the characteristic peak of PS_4^{3-} ions at 420 cm^{-1} in Figure 2b.[38] In the casting and subsequent annealing process, Na_3PS_4 was formed, as shown in eq 1:

$$3Na_2S + P_2S_5 \rightarrow 2Na_3PS_4 \quad (1)$$

After annealing, a shoulder at 380 cm^{-1} appears, which can be ascribed to precipitated Na_2S species.[39,40] Two characteristic peaks detected at around 1590 and 1330 cm^{-1} (Figure S4) were from the G and D bands of graphitic carbon in the CMK-3, respectively.

Figure 2c–f compares the SEM images of the CMK-3 and cast-annealed Na_2S-NPS-C composite cathode after annealed at 270 °C. The CMK-3 shows a rod-like macrostructure with uniform size of 2–3 μm (Figure 2c,d and Figure S5a). After impregnation of Na_2S-Na_3PS_4, the CMK-3 remains the original morphology without any fracture. All of the pores in CMK-3 porous particles were infiltrated by the melting Na_2S-Na_3PS_4 composite due to the capillarity. Apart from the Na_2S-Na_3PS_4 inside the channels of the CMK-3, some Na_2S-Na_3PS_4 composites were also coated on the surface of the mesoporous carbons, forming an ionic conducting network (Figure 2e,f and Figure S5b). These infiltrated CMK-3 particles agglomerated into large particles during the solidification process of melting solid electrolyte between the CMK-3 particles (Figure 2f). The cast-annealed Na_2S-NPS-C in graphite crucible forms a free-standing rod (inset in Figure 2f). The 1D highly ordered channel structure of the CMK-3 with uniform channel diameter of ~4 nm is confirmed by the transition electron microscopy (TEM) images in Figure 3a. After impregnation, almost all of the channels are filled with Na_2S/Na_3PS_4 (Figure 3b). The Na_2S-Na_3PS_4 infiltration dramatically reduces the Brunauer–Emmett–Teller (BET) specific surface area from 1002 m^2/g of CMK-3 to 80 m^2/g of Na_2S-Na_3PS_4-CMK-3, (Figure 3c), and decrease the pore volume from 0.91 cm^3/g of CMK-3 to 0.07 cm^3/g of Na_2S-NPS-C, (Figure 3d). As shown in Figure 3c, the nitrogen adsorption–desorption isotherms of CMK-3 show a typical IV isotherm,[41] presenting a feature of the mesoporous structures with a clear H1 hysteresis loop and narrow mesopore distribution peaks at ~4 nm, in line with the TEM images of the CMK-3 (Figure 3a). After infiltration of the Na_2S/Na_3PS_4 materials into the channel of the carbon, the hysteresis loop disappears, and the mesoporous volume decreases dramatically, indicating the occupying of the Na_2S/Na_3PS_4 in the meso-channels. To further confirm the penetration/infiltration of the Na_2S-Na_3PS_4 in the porous CMK-3, high-angle annular dark-field scanning transmission electron microscopy (HAADF-STEM) with EDX mapping was carried out (Figure 3e,g–j, and Figure S6). The intensity of HAADF-STEM images is proportional to $z^{1.7}$ (z is the atomic number). In Figure 3e, the bright areas correspond to the Na_2S-Na_3PS_4. Even in the less bright area, all of the Na, P, S, and C are totally overlapped, indicating the homogeneous distribution of the Na_2S active species, Na_3PS_4 solid electrolyte, and the mesoporous carbon. Large-scale energy dispersive spectroscopy (EDS) analysis confirms the presence of the carbon, S, P, and Na in all of the composite particles, and all of these elements are ideally overlapped in the composite (Figure S6 and S7); therefore, close contacts among the three components are obtained in the cast-annealed Na_2S-NPS-C nanocomposite. Yet, significant elemental segregation was detected in the ball-milled Na_2S-NPS-C composite (Figure S8), synthesized by ball milling the mixture of Na_2S, Na_3PS_4 and CMK-3 for 1 h. All the characterizations of cast-annealed Na_2S-NPS-C nanocomposite

DOI: 10.1021/acsnano.7b08856
ACS Nano 2018, 12, 3360–3368

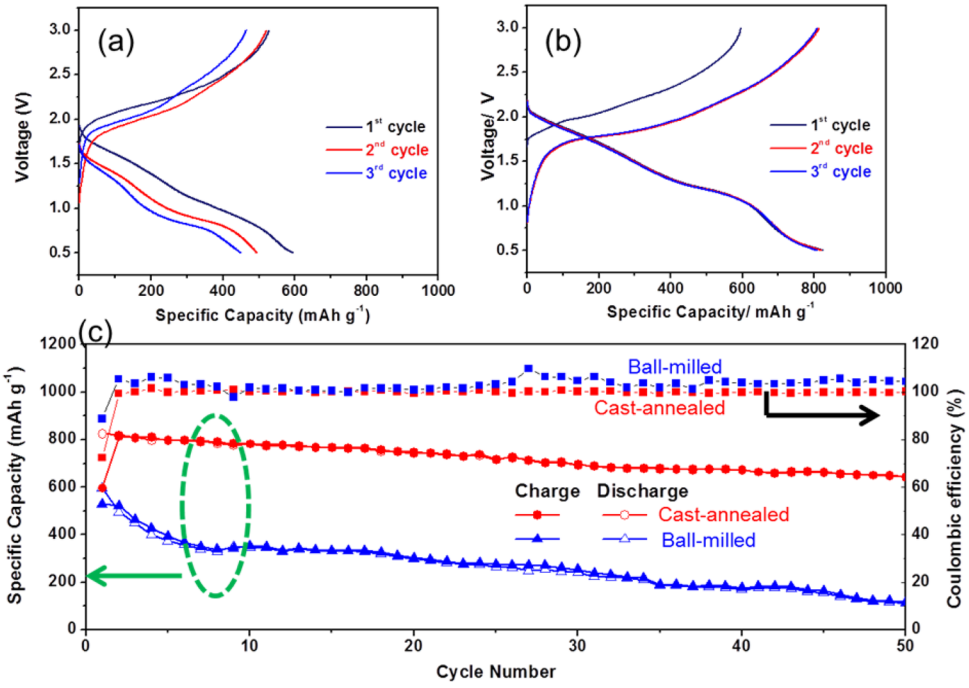

Figure 4. Electrochemical performances of the ball-milled Na_2S-NPS-C composite and cast-annealed Na_2S-NPS-C nanocomposite cathodes in ASNSB tested at 60 °C between 0.5 and 3 V. First three charge−discharge curves of ball-milled Na_2S-NPS-C composite (a) and cast-annealed Na_2S-NPS-C nanocomposite (b) cathodes at 50 mA g^{-1}. (c) Cycling properties of ball-milled Na_2S-NPS-C composite and cast-annealed Na_2S-NPS-C nanocomposite cathodes at a current of 50 mA g^{-1}.

demonstrate that the casting−annealing is a promising technology to synthesize the nanocomposite cathodes for the ASNSBs.

The electrochemical performances of the Na_2S-NPS-C cathodes were evaluated in ASNSBs at 60 °C using $0.75Na_2S{\cdot}0.25P_2S_5$ glass ceramic (Na_3PS_4) as the solid electrolyte and Na−Sn alloy mixed with carbon black as an anode. For reference, the Na_2S-Na_3PS_4-C composite synthesized by ball milling the mixture of Na_2S, Na_3PS_4, and CMK-3 for 1 h was also tested. The utilization of Na−Sn alloy as the anode materials during the battery test could help to lower the interfacial resistance/instability at the anode/solid−electrolyte interface and suppress the detrimental Na dendrites during cycling.[42] Therefore, Na−Sn alloy anodes will not limit the performance of ASNSBs, and the performance differences of ASNSBs using different cathodes are attributed to cathode performance.

The critical challenge for ASNSB is the large volume change (up to 74%) of Na_2S during the S sodiation and desodiation, which dramatically damages the interface contact between Na_2S and Na_3PS_4 and quickly deteriorates the electrochemical performance of the batteries. High performance of all-solid-state Li−S batteries are normally achieved only under the pressure to minimize the impact of volume change of sulfur.[43] To evaluate the robustness of casting−annealing technology, we tested the performance of ASNSB without using spring to apply pressure. Figure 4a presents the charge/discharge profiles of the ball-milled Na_2S-NPS-C composite. The ball-milled Na_2S-NPS-C cathode delivers a discharge capacity of ∼600 mAh/g in the first cycle, accompanying with large overpotential and fast capacity decrease in the subsequent charge/discharge cycles. In contrast, charge/discharge profiles of the cast-annealed Na_2S-NPS-C composite (Figure 4b) provide a significantly higher reversible capacity (>800 mAh/g) with a significantly reduced overpotential to about 1/2 of the ball milled material (Figure 4a). One small plateau at about 0.6 V in the sodiation profile of ball-milled Na_2S-NPS-C and cast-annealed Na_2S-NPS-C cathodes is due to the reduction of P in the Na_3PS_4 solid electrolyte of Na_2S-NPS-C cathode.[44] In the previous investigation, we have shown that certain reversible capacities can be achieved once the Na_3PS_4 solid electrolyte homogeneously mixed with the carbon black.[32] In the cast-annealed composite, the electrolyte also provides about 25% of the total reversible capacities (Figure S9).

Figure 4c compares the cycling properties of the cast-annealed Na_2S-NPS-C and the ball-milled Na_2S-NPS-C cathodes at the same current density of 50 mA/g. The ball-milled Na_2S-NPS-C cathode exhibits a reversible capacity of ∼600 mAh/g for the initial cycle, but the capacity quickly drops to 350 mAh/g after 10 cycles, and further decays to only 110 mAh/g after <50 cycles. In sharp contrast, a much higher discharge capacity of >800 mAh/g is achieved for the cast-annealed Na_2S-NPS-C in the first cycle. After 50 cycles, it still possesses a high reversible capacity of 650 mAh/g, which is about 6 times higher than that of the ball-milled Na_2S-NPS-C cathode. The cast-annealed Na_2S-NPS-C shows the best electrochemical performance in all reported nano-Na_2S/Na_3PS_4/C cathodes.[32,33] The high reversible capacity of >650 mAh/g at the average discharge potential of 1.3 V provides an energy density of >800 Wh/kg. This value is even higher than that of the present high-temperature (>300 °C) Na−S batteries (760 Wh/kg). The cast-annealed Na_2S-NPS-C nanocomposite cathodes also show a high Coulombic efficiency (∼100%) without any shuttle reactions. Besides, the electrochemical performance of the ASNSB using cast-annealed Na_2S-NPS-C cathodes is also much better than that of the Na−S batteries based on the polymer or ether electrolytes, which only shows low capacities of <400 mAh/g with limited cycling performance

DOI: 10.1021/acsnano.7b08856
ACS Nano 2018, 12, 3360−3368

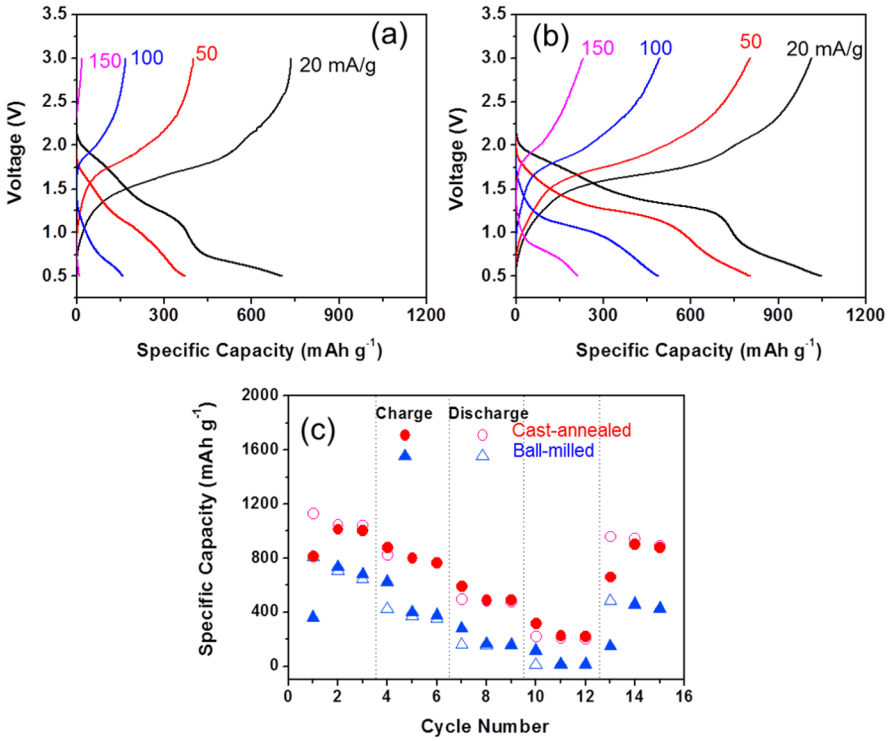

Figure 5. Charge−discharge profiles of the ball-milled Na_2S-NPS-C composite (a) and cast-annealed Na_2S-NPS-C nanocomposite (b) cathodes in the ASNSB at 60 °C between 0.5 and 3 V at different current densities from 20 mA g^{-1} to 150 mA g^{-1}. The cells were precycled for 3 cycles at each current density, and the second charge−discharge profiles were provided. (c) Rate performance of ball-milled Na_2S-NPS-C composite and cast-annealed Na_2S-NPS-C cathodes in the ASSB at 60 °C between 0.5 and 3 V.

(<10 cycles).[24,27] The significant capacity decay for the ball milled sample could be due to the dramatic increase of the interfacial resistance as confirmed by the continuous increase of the overpotential (Figure 4a). The resistances of ball-milled Na_2S-NPS-C cathode and cast-annealed Na_2S-NPS-C cathode at different charge/discharge cycles were measured using electrochemical impedance spectroscopy (EIS). Figure S10 shows the EIS of two cathodes at the fully discharged state at 1, 10, 30, and 50th cycles. The semicircles in the Nyquist plots represent the interfacial resistances, whereas the low-frequency slope line is ascribed to the sodium ions diffusion inside the cathodes. The cast-annealed Na_2S-NPS-C cathode exhibits a much lower interfacial resistance than that of the ball milled Na_2S-NPS-C composite cathode. The dramatically decreased interfacial resistance between the active species of the electrolyte benefits from the intimate contacts among Na_2S, Na_3PS_4 solid electrolyte, and the CMK-3 electron conducting agent. Although the interface resistances of both two cathodes increase due to large volume change of Na_2S and lack of pressure to recover the volumetric change during repeated sodiation/desodiation reactions, the amount of resistance increase of the cast-annealed Na_2S-NPS-C cathode is much smaller than that of the ball-milled Na_2S-NPS-C composites (Figure S10), demonstrating high robustness of cast-annealed materials. Moreover, a high Coulombic efficiency of ∼100% was obtained after second cycles for the cast-annealed Na_2S-NPS-C cathode, implying the excellent reversibility of the sodiation/desodiation process and the total suppression of the polysulfide shuttle reactions. The polysulfide shuttle was proven to be the key challenge for the room-temperature liquid electrolytes Na−S batteries.[24]

The cast-annealed Na_2S-NPS-C cathode also exhibits a significantly improved kinetics with a much lower voltage hysteresis than that of the ball-milled Na_2S-NPS-C composite at room temperature (Figure S11). The rate capabilities of the ball-milled Na_2S-NPS-C cathode and the cast-annealed Na_2S-Na_3PS_4-CMK-3 cathode were also tested at 60 °C by enlarging the current density from 20 to 150 mA/g. Figure 5a,b compares the sodiation/desodiation profiles of these two different cathodes at different current densities, and Figure 5c shows their rate capacities. For the ball-milled Na_2S-NPS-C composite, only a reversible capacity of ∼150 mAh/g can be achieved at a current of 100 mA/g. As the current density is raised to 150 mA/g, the reversible capacity dramatically decays to <10 mAh/g. However, for cast-annealed Na_2S-NPS-C cathode, high capacities of 1050, 750, 500, and 200 mAh/g can be achieved at a charge−discharge current of 20, 50, 100, and 150 mA/g, respectively. Moreover, once the current density is finally decreased back to 20 mA/g, the capacity could return to ∼900 mAh/g, indicating the good tolerance for the volume change for cast-annealed Na_2S-NPS-C cathode during the rapid sodiation/desodiation reactions.

For the Li-ion batteries using fluid liquid or gel electrolyte, only the electronic conductivity and porosity of the cathode should be designed, because the infiltrative liquid/gel electrolyte could provide high ionic conductivity, low interface resistance, and high capability to accommodate the volume change. However, for the inorganic solid-state batteries, all of these electron and ion conductions, interface resistances, and mechanical properties for accommodation of volume change have to be carefully designed. To realize a high performance of all-inorganic solid-state batteries, the following requirements should be satisfied: (1) Nanosized active materials should be

DOI: 10.1021/acsnano.7b08856
ACS Nano 2018, 12, 3360−3368

uniformly distributed and lattice matched to the ceramic electrolyte matrix, forming effective ion conducting channels. (2) Meanwhile, the electronic conductive nanoscaled network should be formed in the cathode side. (3) The cathode should have high mechanical strength and robustness to tolerate the huge stress and volume change. Such a structure and property have not been fabricated by scientists and engineers in the battery community. Herein, using Na−S as a model cell, we fabricated such type of cast-annealed Na_2S-NPS-C cathodes using casting−annealing approach, in which all of these requirements are met at the same time, therefore improved electrochemical properties with a high active material utilization in our ASNSB was realized.

CONCLUSION

In summary, a high-performance all-inorganic solid-state Na−S battery (ASNSB) with cast-annealed Na_2S-NPS-C nanocomposite cathode was synthesized *via* a casting−annealing process that has been widely used in structural materials. We first heat the Na_2S-P_2S_5-CMK-3 above into liquid (680 °C), allowing liquid Na_2S-Na_3PS_4 to penetrate into porous CMK-3, and then quench it to room temperature forming Na_2S saturated Na−P−S glass filled CMK-3 composite, where Na−P−S glass has intimate contact with carbon. During the followed annealing process, Na_2S nanoparticles are precipitated from Na−P−S glass matrix, forming a crystal Na_2S-Na_3PS_4-C nanocomposite with stable interfacial contact and free stress. The Na_3PS_4 with precipitated Na_2S was evenly mixed in the mesoporous carbon matrix, significantly enhancing the mechanical and ion and electron conductivity of the cast-annealed Na_2S-NPS-C nanocomposite cathodes. The ASNSB using the cast-annealed Na_2S-NPS-C nanocomposite as the cathode delivered a high reversible capacity of ∼650 mAh/g for 50 cycles at a relatively low temperature of 60 °C. The superior electrochemical performance using the low-cost raw materials with facile and sustainable synthesis of Na_2S-Na_3PS_4-CMK-3 for the low-temperature ASNSBs is an attractive approach toward promoting Na−S batteries at industrial scale. Moreover, it should be pointed out that the present casting method, which translates the traditional particle-to-particle contact in solid battery to interfacial contact, should be a general and scalable strategy to design other robust and high electrochemical performance all-solid-state batteries.

EXPERIMENTAL SECTION

Sample Synthesis. Na_2S and P_2S_5 (99%) powders were bought from Sigma-Aldrich. Ordered mesoporous carbon of CMK-3 was bought from ACS Material, LLC. Na_3PS_4 solid electrolyte was synthesized by ball milling following an annealing process based on the previous reports.[38,42] The cast-annealed Na_2S-NPS-C cathode composite was synthesized by casting−annealing method. First, the starting materials of Na_2S, P_2S_5 and CMK-3 mesoporous carbon were hand milled with mortar and pestle in the glovebox. Here, the weight ratio of Na_2S:P_2S_5:CMK-3 was set as 50.5:19.5:30 to make sure the weight ratio of Na_2S, Na_3PS_4, and porous carbon in final Na_2S/Na_3PS_4/CMK-3 cathode composite is 30:40:30. It should be pointed out that based on the Na_2S-P_2S_5 phase diagram, different ratios of Na_2S and Na_3PS_4 can be synthesized by adjusting the ratio of the starting materials of Na_2S and P_2S_5. The mixtures were then transferred into a graphite crucible, which was put into a clear quartz tube and sealed under vacuum. The tube was raised to 850 °C with a ramping rate of 2 °C/min and kept for 1 h. After the temperature was raised to higher than the liquidus, the Na_2S and P_2S_5 will melt with each other, forming a homogeneous liquid. After that, the quartz tube was immediately transferred into the ice water and quenched to 0 °C in 10 s. Due to the fast temperature drop, the amorphous state of the liquid was kept at room temperature. After quenching, the quartz tube was put in the oven and annealed at 270 °C for 2 h. After cooling down to 25 °C, the cast-annealed Na_2S-NPS-C composite was taken out from the quartz tube in the glovebox. For the reference, the ball-milled Na_2S-NPS-C with the same mass rate was also prepared by ball milling the Na_2S, Na_3PS_4, and CMK-3 mixture at a fixed rotation speed of 370 rpm for 1 h.

Characterization. X-ray diffraction (XRD) was performed on a Bruker Smart1000 diffractometer with a Cu Kα radiation. Scanning electron microscopy (SEM, Hitachi SU-70, Japan) and transmission electron microscopy (TEM, JEM 2100 LaB_6, 200 keV) were utilized to characterize the morphology and microstructure of the samples. N_2 adsorption by means of a Micromeritics ASAP 2020 Porosimeter Test Station was adopted to get the information on the specific surface areas, pore volumes, and related pore size distributions of the samples. Before characterization, all of the samples were evacuated and degassed at 180 °C for 12 h. The specific surface areas of the samples were obtained using the Brunauer−Emmett−Teller (BET) method. The Barrett−Joyner−Halenda (BJH) equation was utilized to get the porosity distribution of the samples. Raman spectra were tested on a Horiba Jobin Yvon Labram Aramis with a 532 nm diode-pumped solid-state laser.

Electrochemical Measurements. The all-inorganic solid-state Na−S batteries were fabricated using the as-obtained composite as working electrode and Na_3PS_4 as the solid electrolyte. Na metal is highly reactive to the sulfide solid electrolyte to form the Na_2S and Na_3P. The *in situ* formed Na_2S and Na_3P interphases will dramatically increase the interfacial resistance between Na anode and Na_3PS_4. Besides, the Na dendrites also grow in the solid-state electrolyte if Na metal was utilized as the anode. Therefore, a Na−Sn−C composite was adopted as the reference and anode electrode (Figure S12). The ionic conductivities of Na_3PS_4 solid electrolyte were measured in an ion-blocking Pt/Na_3PS_4/Pt cell using EIS at 25 and 60 °C. The ion-blocking Pt/Na_3PS_4/Pt cell was prepared by cold pressing of 150 mg of Na_3PS_4, followed by Pt sputtering. The ion conductivity of the Na_3PS_4 calculated from the EIS profiles (Figure S13) is 1.43×10^{-4} S/cm at 25 °C. At a high temperature of 60 °C, the conductivity is increased to 3.45×10^{-4} S/cm. The Na−Sn−C composite was prepared according to previous literature.[45] To assemble the cell, the cast-annealed or ball-milled Na_2S-NPS-C powders (5 mg) composite cathodes were put on one side of the Na_3PS_4 solid electrolyte (120 mg) in a PTFE tank. The diameter of the PTFE tank is 10 mm, and Na−Sn−C anode powders (100 mg) were placed on the other side of the solid electrolyte membrane and then pressed together. The applied pressure between two stainless steel rods is 360 MPa. Galvanostatic discharge−charge cycles were conducted using a battery cycler (LAND CT-2001A, China) with a voltage range of 0.5−3.0 V at 60 °C. It should be pointed out that there is no extra pressure applied during the battery test. The specific capacities and current densities were calculated based on the mass of active material (Na_2S). The ratio of Na_2S to Na_3PS_4 was calculated based on the lever rule in the phase diagram. EIS was obtained by an electrochemistry workstation (Solatron 1287/1260) over a range from 1×10^5 Hz to 0.1 Hz, with an AC amplitude of 0.02 V.

ASSOCIATED CONTENT

Supporting Information

The Supporting Information is available free of charge on the ACS Publications website at DOI: 10.1021/acsnano.7b08856.

Digital image of the synthesis tube, XRD patterns, SEM and corresponding EDS results, electrochemical performance at room temperature (Figures S1−S13) (PDF)

AUTHOR INFORMATION

Corresponding Author

*E-mail: cswang@umd.edu.

DOI: 10.1021/acsnano.7b08856
ACS Nano 2018, 12, 3360−3368

ORCID

Ji Chen: 0000-0003-0326-8304
Xiuquan Zhou: 0000-0002-1361-3880
Chunsheng Wang: 0000-0002-8626-6381

Author Contributions

[§]These authors contributed equally to this work.

Notes

The authors declare no competing financial interest.

ACKNOWLEDGMENTS

The authors acknowledge the support by Army Research Lab under award number W911NF1510187. The authors really appreciate the support of the Maryland NanoCenter and its NispLab.

REFERENCES

(1) Dunn, B.; Kamath, H.; Tarascon, J.-M. Electrical Energy Storage for the Grid: A Battery of Choices. *Science* **2011**, *334*, 928−935.

(2) Divya, K. C.; Østergaard, J. Battery Energy Storage Technology for Power Systems-An Overview. *Electr. Power Syst. Res.* **2009**, *79*, 511−520.

(3) Armand, M.; Tarascon, J. M. Building Better Batteries. *Nature* **2008**, *451*, 652−657.

(4) Tarascon, J.-M. Is Lithium the New Gold? *Nat. Chem.* **2010**, *2*, 510.

(5) Ellis, B. L.; Nazar, L. F. Sodium and Sodium-Ion Energy Storage Batteries. *Curr. Opin. Solid State Mater. Sci.* **2012**, *16*, 168−177.

(6) Kim, I.; Park, J.-Y.; Kim, C. H.; Park, J.-W.; Ahn, J.-P.; Ahn, J.-H.; Kim, K.-W.; Ahn, H.-J. A Room Temperature Na/S Battery Using a β'' Alumina Solid Electrolyte Separator, Tetraethylene Glycol Dimethyl Ether Electrolyte, and a S/C Composite Cathode. *J. Power Sources* **2016**, *301*, 332−337.

(7) Lu, X.; Xia, G.; Lemmon, J. P.; Yang, Z. Advanced Materials for Sodium-Beta Alumina Batteries: Status, Challenges and Perspectives. *J. Power Sources* **2010**, *195*, 2431−2442.

(8) Wen, Z.; Cao, J.; Gu, Z.; Xu, X.; Zhang, F.; Lin, Z. Research on Sodium Sulfur Battery for Energy Storage. *Solid State Ionics* **2008**, *179*, 1697−1701.

(9) Nagata, H.; Chikusa, Y. An All-Solid-State Sodium−Sulfur Battery Operating at Room Temperature Using a High-Sulfur-Content Positive Composite Electrode. *Chem. Lett.* **2014**, *43*, 1333−1334.

(10) Larcher, D.; Tarascon, J. M. Towards Greener and More Sustainable Batteries for Electrical Energy Storage. *Nat. Chem.* **2015**, *7*, 19−29.

(11) Xin, S.; Yin, Y.-X.; Guo, Y.-G.; Wan, L.-J. A High-Energy Room-Temperature Sodium-Sulfur Battery. *Adv. Mater.* **2014**, *26*, 1261−1265.

(12) Lu, X.; Kirby, B. W.; Xu, W.; Li, G.; Kim, J. Y.; Lemmon, J. P.; Sprenkle, V. L.; Yang, Z. Advanced Intermediate-Temperature Na-S Battery. *Energy Environ. Sci.* **2013**, *6*, 299−306.

(13) Ji, X.; Lee, K. T.; Nazar, L. F. A Highly Ordered Nanostructured Carbon-Sulphur Cathode for Lithium-Sulphur Batteries. *Nat. Mater.* **2009**, *8*, 500−506.

(14) Fan, L.; Ma, R.; Yang, Y.; Chen, S.; Lu, B. Covalent Sulfur for Advanced Room Temperature Sodium-Sulfur Batteries. *Nano Energy* **2016**, *28*, 304−310.

(15) Carter, R.; Oakes, L.; Douglas, A.; Muralidharan, N.; Cohn, A. P.; Pint, C. L. A Sugar-Derived Room-Temperature Sodium Sulfur Battery with Long Term Cycling Stability. *Nano Lett.* **2017**, *17*, 1863−1869.

(16) Yu, X.; Manthiram, A. Na_2S-Carbon Nanotube Fabric Electrodes for Room-Temperature Sodium−Sulfur Batteries. *Chem. - Eur. J.* **2015**, *21*, 4233−4237.

(17) Wei, S.; Xu, S.; Agrawral, A.; Choudhury, S.; Lu, Y.; Tu, Z.; Ma, L.; Archer, L. A. A Stable Room-Temperature Sodium−Sulfur Battery. *Nat. Commun.* **2016**, *7*, 11722.

(18) Kim, I.; Kim, C. H.; Choi, S. h.; Ahn, J.-P.; Ahn, J.-H.; Kim, K.-W.; Cairns, E. J.; Ahn, H.-J. A Singular Flexible Cathode for Room Temperature Sodium/Sulfur Battery. *J. Power Sources* **2016**, *307*, 31−37.

(19) Kim, S. I.; Park, W. I.; Jung, K.; Kim, C.-S. An Innovative Electronically-Conducting Matrix of the Cathode for Sodium Sulfur Battery. *J. Power Sources* **2016**, *320*, 37−42.

(20) Yu, X.; Manthiram, A. Performance Enhancement and Mechanistic Studies of Room-Temperature Sodium−Sulfur Batteries with a Carbon-Coated Functional Nafion Separator and a Na_2S/Activated Carbon Nanofiber Cathode. *Chem. Mater.* **2016**, *28*, 896−905.

(21) Wang, Y.-X.; Yang, J.; Lai, W.; Chou, S.-L.; Gu, Q.-F.; Liu, H. K.; Zhao, D.; Dou, S. X. Achieving High-Performance Room-Temperature Sodium−Sulfur Batteries With S@Interconnected Mesoporous Carbon Hollow Nanospheres. *J. Am. Chem. Soc.* **2016**, *138*, 16576−16579.

(22) Kohl, M.; Borrmann, F.; Althues, H.; Kaskel, S. Hard Carbon Anodes and Novel Electrolytes for Long-Cycle-Life Room Temperature Sodium-Sulfur Full Cell Batteries. *Adv. Energy Mater.* **2016**, *6*, 1502185.

(23) Chen, Y.-M.; Liang, W.; Li, S.; Zou, F.; Bhaway, S. M.; Qiang, Z.; Gao, M.; Vogt, B. D.; Zhu, Y. A Nitrogen Doped Carbonized Metal-Organic Framework for High Stability Room Temperature Sodium-Sulfur Batteries. *J. Mater. Chem. A* **2016**, *4*, 12471−12478.

(24) Ryu, H.; Kim, T.; Kim, K.; Ahn, J.-H.; Nam, T.; Wang, G.; Ahn, H.-J. Discharge Reaction Mechanism of Room-Temperature Sodium-Sulfur Battery with Tetra Ethylene Glycol Dimethyl Ether Liquid Electrolyte. *J. Power Sources* **2011**, *196*, 5186−5190.

(25) Wang, J.; Yang, J.; Nuli, Y.; Holze, R. Room Temperature Na/S Batteries with Sulfur Composite Cathode Materials. *Electrochem. Commun.* **2007**, *9*, 31−34.

(26) Kim, J.-S.; Ahn, H.-J.; Kim, I.-P.; Kim, K.-W.; Ahn, J.-H.; Park, C.-W.; Ryu, H.-S. The Short-Term Cycling Properties of Na/PVdF/S Battery at Ambient Temperature. *J. Solid State Electrochem.* **2008**, *12*, 861−865.

(27) Park, C.-W.; Ryu, H.-S.; Kim, K.-W.; Ahn, J.-H.; Lee, J.-Y.; Ahn, H.-J. Discharge Properties of All-Solid Sodium−Sulfur Battery Using Poly (ethylene oxide) Electrolyte. *J. Power Sources* **2007**, *165*, 450−454.

(28) Yu, X.; Manthiram, A. Capacity Enhancement and Discharge Mechanisms of Room-Temperature Sodium−Sulfur Batteries. *ChemElectroChem* **2014**, *1*, 1275−1280.

(29) Wang, Y.-X.; Zhang, B.; Lai, W.; Xu, Y.; Chou, S.-L.; Liu, H.-K.; Dou, S.-X. Room-Temperature Sodium-Sulfur Batteries: A Comprehensive Review on Research Progress and Cell Chemistry. *Adv. Energy Mater.* **2017**, *7*, 1602829.

(30) Tanibata, N.; Deguchi, M.; Hayashi, A.; Tatsumisago, M. All-Solid-State Na/S Batteries with a Na_3PS_4 Electrolyte Operating at Room Temperature. *Chem. Mater.* **2017**, *29*, 5232−5238.

(31) Han, F.; Yue, J.; Fan, X.; Gao, T.; Luo, C.; Ma, Z.; Suo, L.; Wang, C. High-Performance All-Solid-State Lithium−Sulfur Battery Enabled by a Mixed-Conductive Li_2S Nanocomposite. *Nano Lett.* **2016**, *16*, 4521−4527.

(32) Yue, J.; Han, F.; Fan, X.; Zhu, X.; Ma, Z.; Yang, J.; Wang, C. High-Performance All-Inorganic Solid-State Sodium−Sulfur Battery. *ACS Nano* **2017**, *11*, 4885−4891.

(33) Tanibata, N.; Tsukasaki, H.; Deguchi, M.; Mori, S.; Hayashi, A.; Tatsumisago, M. Characterization of Sulfur Nanocomposite Electrodes Containing Phosphorus Sulfide for High-Capacity All-Solid-State Na/S Batteries. *Solid State Ionics* **2017**, *311*, 6−13.

(34) Wang, Q. G.; Davidson, C. J. Solidification and Precipitation Behaviour of Al-Si-Mg Casting Alloys. *J. Mater. Sci.* **2001**, *36*, 739−750.

(35) Yanagihara, E.; Orii, S.; Iketani, T.; Saikawa, S.; Matsuda, K.; Ikeno, S. Precipitation Structure of Al-10 mass%Si-0.3 mass% Mg Alloy Produced by High Pressure Die Casting and Permanent Mold Casting with T5 Treatment. *Mater. Trans.* **2015**, *56*, 1112−1119.

DOI: 10.1021/acsnano.7b08856
ACS Nano 2018, 12, 3360−3368

(36) *Alloy Phase Diagram Database*. ASM International: Materials Park, OH, http://mio.asminternational.org/apd/index.aspx (accessed Dec. 10, 2017).
(37) Ridgway, P. L.; McLarnon, F. R.; Cairns, E. J. Sodium/Phosphorus-Sulfur Cells: II. Phase Equilibria. *J. Electrochem. Soc.* **1996**, *143*, 412−417.
(38) Noi, K.; Hayashi, A.; Tatsumisago, M. Structure and Properties of the Na_2S-P_2S_5 Glasses and Glass−Ceramics Prepared by Mechanical Milling. *J. Power Sources* **2014**, *269*, 260−265.
(39) Seh, Z. W.; Yu, J. H.; Li, W.; Hsu, P.-C.; Wang, H.; Sun, Y.; Yao, H.; Zhang, Q.; Cui, Y. Two-Dimensional Layered Transition Metal Disulphides for Effective Encapsulation of High-Capacity Lithium Sulphide Cathodes. *Nat. Commun.* **2014**, *5*, 5017.
(40) Lin, Z.; Liu, Z.; Dudney, N. J.; Liang, C. Lithium Superionic Sulfide Cathode for All-Solid Lithium−Sulfur Batteries. *ACS Nano* **2013**, *7*, 2829−2833.
(41) Li, W.; Yang, Z.; Li, M.; Jiang, Y.; Wei, X.; Zhong, X.; Gu, L.; Yu, Y. Amorphous Red Phosphorus Embedded in Highly Ordered Mesoporous Carbon with Superior Lithium and Sodium Storage Capacity. *Nano Lett.* **2016**, *16*, 1546−1553.
(42) Hayashi, A.; Noi, K.; Sakuda, A.; Tatsumisago, M. Superionic Glass-Ceramic Electrolytes for Room-Temperature Rechargeable Sodium Batteries. *Nat. Commun.* **2012**, *3*, 856.
(43) Yao, X.; Huang, N.; Han, F.; Zhang, Q.; Wan, H.; Mwizerwa, J. P.; Wang, C.; Xu, X. High-Performance All-Solid-State Lithium−Sulfur Batteries Enabled by Amorphous Sulfur-Coated Reduced Graphene Oxide Cathodes. *Adv. Energy Mater.* **2017**, *7*, 1602923.
(44) Chu, I.-H.; Kompella, C. S.; Nguyen, H.; Zhu, Z.; Hy, S.; Deng, Z.; Meng, Y. S.; Ong, S. P. Room-Temperature All-Solid-State Rechargeable Sodium-Ion Batteries with a Cl-Doped Na_3PS_4 Superionic Conductor. *Sci. Rep.* **2016**, *6*, 33733.
(45) Hayashi, A.; Noi, K.; Tanibata, N.; Nagao, M.; Tatsumisago, M. High Sodium Ion Conductivity of Glass−Ceramic Electrolytes with Cubic Na_3PS_4. *J. Power Sources* **2014**, *258*, 420−423.

DOI: 10.1021/acsnano.7b08856
ACS Nano 2018, 12, 3360−3368